Int. J. Heat Mass Transfer. Vol. 34, No. 4/5, pp. 929–940, 1991
Printed in Great Britain

0017–9310/91 $3.00 + 0.00

Direct simulation of wave interactions in unsteady natural convection in a cavity

S. W. ARMFIELD and JOHN C. PATTERSON
Centre for Water Research, University of Western Australia, Nedlands, WA 6009, Australia

(*Received* 3 *November* 1989 *and in final form* 2 *April* 1990)

Abstract—Numerical solutions for unsteady natural convection flow in a square cavity with differentially heated side walls are obtained using an implicit second-order time-accurate finite volume scheme, and briefly compared to experimental data reported elsewhere. The results predict the occurrence of a cavity scale seiche, the presence of waves in the vertical thermal boundary layer that travel from the walls into the horizontal intrusions that form on the horizontal boundaries, and a region of strong divergence at the upstream end of the intrusions. These three mechanisms are observed to interact at a Rayleigh number of 5×10^9 to produce a mixing patch in the intrusion, suggestive of a transition to turbulence. The net heat transfer and the approach to steady state are strongly influenced by the presence of the waves.

1. INTRODUCTION

NATURAL convection in rectangular cavities with unequally heated side walls is a problem of fundamental interest to fluid mechanics and heat transfer, with many geophysical and industrial applications. In many cases, the application of the side heating is unsteady in some sense, and the transient response of the system is of some importance, particularly in the start-up period following a sudden change in side wall temperature. This problem was first addressed in ref. [1], with numerical simulations and scaling analyses of cases with Rayleigh numbers up to 1.4×10^5. One of the important results of that paper was the apparent presence of a decaying oscillatory approach to steady state in certain Rayleigh number regimes, at a frequency which was consistent with the first mode cavity scale internal wave (seiche) based on a linear vertical stratification in the cavity. The oscillatory behaviour was particularly evident in the measure of the net heat transfer across the cavity. This result was supported by other numerical results (e.g. refs. [2–4]), although experimental support was not available until the experiments of Patterson and Armfield [5] showed some evidence of the oscillatory behaviour.

The specific problem considered in all of these cases was that of an isothermal (at temperature T_m), stationary fluid in a square cavity. At time $t = 0$ the vertical walls were instantaneously heated and cooled to $T_m \pm \Delta T/2$. Briefly, the flow that evolved consisted of narrow boundary layers on the vertical walls exiting into the cavity at the downstream corners in heated and cooled intrusions. These intrusions filled the cavity, resulting in a nearly linear stratification in the core at steady state. The experiments of Ivey [6], although showing no evidence of the cavity scale waves, revealed the existence of a rapid flow divergence near the upstream end of the intrusions. Ivey likened this to an internal hydraulic jump, based on the calculation of a densimetric Froude number for the inflowing intrusion which was greater than one. Further, high frequency temperature signals were observed in the intrusion and were associated by Paolucci and Chenoweth [7] with the downstream wave train shed by an undular jump with Froude number near one. Paolucci and Chenoweth, although dealing with a flow generated by perturbing a steady flow with an increase in Rayleigh number, also observed the cavity scale seiching, but suggested a different generation mechanism to that of ref. [1]. In a similar numerical analysis, LeQuere and Alziary de Roquefort [8] observed the presence of travelling waves which resulted in a steady periodic flow; the waves were initiated as a thermal boundary layer instability which travelled up (or down) the vertical layers, across the intrusions, and into the opposing layers. These waves were also described in ref. [7], where for sufficiently high Rayleigh numbers it was found that the waves became unstable and chaotic flow resulted. These waves are evidently of the thermally driven type identified by Gill and Davey [9].

The first experimental observation of these travelling waves in the context of the side heated cavity was described in ref. [5]. In ref. [5] a joint numerical and experimental investigation showed that the instabilities were generated in the initially stationary case by, first, the start-up of the thermal boundary layer, and second, the horizontal intrusion reaching the opposing thermal boundary layer. This second event also triggered the cavity scale seiching. The presence of the rapid flow divergence near the upstream ends of the exiting intrusions was confirmed, although this existed for flows for which the Froude number was less than one, suggesting that a mechanism other than an internal hydraulic jump in the usual sense was responsible. An alternative generation mechanism resulting from a conduction blocking effect is given in ref. [5]. However, many of the features observed were

NOMENCLATURE

g	acceleration due to gravity	V	y-velocity component
Gr	Grashof number, Ra/Pr	x	horizontal distance from bottom left corner of cavity
H	height of cavity	y	vertical distance from bottom left corner of cavity.
Pr	Prandtl number, ν/κ		
Ra	Rayleigh number, $g\beta H^3(\Delta T)/\nu\kappa$		
t	time		
T	temperature	Greek symbols	
T_m	mean temperature	β	coefficient of thermal expansion
ΔT	total temperature variation in cavity	δ_t	thermal boundary layer thickness
U	x-velocity component	κ	thermal conductivity
v	velocity	ν	kinematic viscosity.

similar to those of a jump, and the analogy is a useful one.

In this paper the presence of the travelling waves, the internal seiche, and the presence of the rapid flow divergence are considered in some detail by means of numerical simulation. For brevity, only results for Rayleigh numbers (Ra) of 6×10^8 and 5×10^9 are presented. In the higher Ra case, the interaction of the cavity scale wave with the diverging flow generates a patch of mixing fluid in the region of the divergence, suggestive of transition to turbulence. This feature is not present in the lower Ra case, which is used to demonstrate the presence of the cavity scale seiche. In both cases, the flow divergence in the intrusion is present, although only in the upper Ra value is the intrusion Froude number greater than one. In the following, the numerical method is described in Section 2, and the numerical results are presented in Section 3, including a brief comparison with experimental data. Temperature contours are used to demonstrate the presence of the waves and the flow divergence, and spectra from temperature traces indicate the actual frequencies. In Section 4, the mechanisms for the generation of the various waves and their effects are identified and the implications discussed.

2. NUMERICAL METHOD

The governing equations are the Navier–Stokes equations and the temperature equation, with the Boussinesq assumption allowing the incompressible form of the equations to be used. The equations are written in conservative non-dimensional form as

$$U_t+(UU)_x+(VU)_y=-P_x+(U_{xx}+U_{yy}) \quad (1)$$

$$V_t+(UV)_x+(VV)_y=-P_y+(V_{xx}+V_{yy})+\frac{Ra\,T}{Pr} \quad (2)$$

$$U_x+V_y=0 \quad (3)$$

$$T_t+(UT)_x+(VT)_y=\frac{1}{Pr}(T_{xx}+T_{yy}) \quad (4)$$

where subscripts denote partial differentiation. In these equations, velocity is nondimensionalized by ν/H, time by H^2/ν, length by H, and the temperature relative to T_m by ΔT.

2.1. *Boundary conditions*

The top and bottom of the cavity are insulated and all boundaries are non-slip. Initially the fluid is at rest and isothermal ($T=0$) and at $t=0$ the side walls are heated and cooled impulsively to non-dimensional temperatures $\pm\frac{1}{2}$.

2.2. *Discretization*

Because of the large variation in length scales it is necessary to use a mesh that concentrates points in the boundary layer and is relatively coarse in the interior. In the $Ra=6\times10^8$ flow the point nearest the wall is located one thousandth of a cavity width in from the wall, with the mesh then expanding at a rate of 10% until the edge of the thermal boundary layer is reached, resulting in approximately an 80×80 mesh. Extensive grid and time step dependency tests have been conducted for the lower Rayleigh number flow. Reducing the wall mesh size to one four thousandth of the cavity width, and the time step by one half, has been found to give identical results for this Rayleigh number [5]. Owing to the long computation times required for the higher Rayleigh number such extensive testing has not been possible. The time step used for the higher Rayleigh number is one tenth that of the lower Rayleigh number, while the wall mesh size is one half.

The equations are discretized on a non-staggered mesh in which all variables are stored at the same grid locations. The method of obtaining the pressure and satisfying continuity is similar to the SIMPLE schemes used with the conventional staggered mesh [10]. To enable this approach to be used with a non-staggered mesh regularizing terms are included in the Poisson equation for the pressure. Without the inclusion of these regularizing terms the scheme would lead to an odd–even splitting of the pressure, with a resulting degradation and ultimate collapse of the solution. The regularizing terms have the effect of

ensuring the discrete scheme is strongly elliptic, while without them the scheme is non-elliptic. Comparisons between staggered and non-staggered solutions indicate both schemes have an equivalent accuracy [11]. The advantage of using the non-staggered scheme is that all variables have the same discrete operators. With a staggered non-uniform mesh a different operator must be used for each of the velocities and the scalar variables. Hence the use of the non-staggered approach leads to a considerable saving in programming and computer time. This scheme is described in detail in ref. [11].

Finite volumes are used to convert differential terms in the governing equations to differences as follows. All second derivatives and linear first derivatives are approximated by second-order central differences. The convective terms are approximated by a QUICK scheme, which with the implicit method used gives equivalent accuracy to QUICKEST used with an explicit method [12]. All non-linear terms are centrally differenced with respect to time.

The discretization produces the usual fringed block tridiagonal matrix operator, one for each of the momentum, temperature and pressure equations. These are solved using an alternating direction Gauss–Seidel iterative method. At each time step an initial estimate for the unknown quantity is obtained by making a quadratic extrapolation from the two previous time steps.

2.3. *Time integration*

The time integration scheme is a second-order Crank–Nicholson predictor–corrector method in which the solution of the transport equations is carried out in the following way. First, all variables are known at time $t = n\Delta t$ where Δt is the time step. Second the heat equation (4) is inverted to obtain an initial approximation to T^{n+1}, and using this value the two momentum equations (1) and (2) are inverted, using an estimated pressure field, to obtain a first approximation to U^{n+1} and V^{n+1}. A pressure correction equation derived from equation (3) is then solved to enforce continuity. Finally new estimates of U^{n+1} and V^{n+1} are obtained. This procedure is repeated until a preset convergence criterion is attained.

3. RESULTS

Results are presented for Rayleigh numbers of 6×10^8 and 5×10^9, and Prandtl number of 7. All distances, times, and temperatures are nondimensional as defined above. In all cases the hot wall is on the right, and distances are measured relative to the lower left corner, that is the downstream end of the cold wall. In general, the discussion of results will be presented in terms of the hot wall and the hot intrusion; the cold wall and cold intrusion are symmetric about the central point of the cavity. In all temperature contour figures, 20 contours equally spaced between $\pm \frac{1}{2}$ are shown. The code has been run on the Centre for Water Research long instruction word Culler mini–super computer. On this machine the code runs at about 30 times the speed of a typical 68020/68881 machine such as a SUN 3/50. Run times are of the order of 18 h for the lower Rayleigh number and 5 days for the higher Rayleigh number.

The presence of travelling waves in the vertical thermal boundary layers are shown in Fig. 1. Here the simulated temperature contours are shown for both cases at particular times ($Ra = 6 \times 10^8$, $t = 2.8 \times 10^{-3}$,

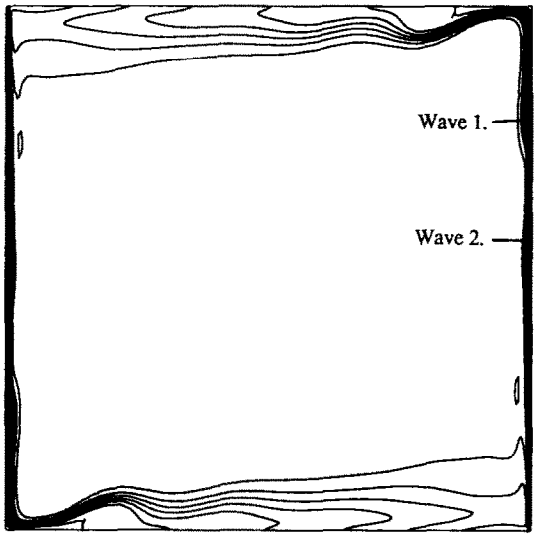

FIG. 1(a). Simulated non-dimensional temperature contours for $Ra = 6 \times 10^8$ at non-dimensional time $t = 2.8 \times 10^{-3}$.

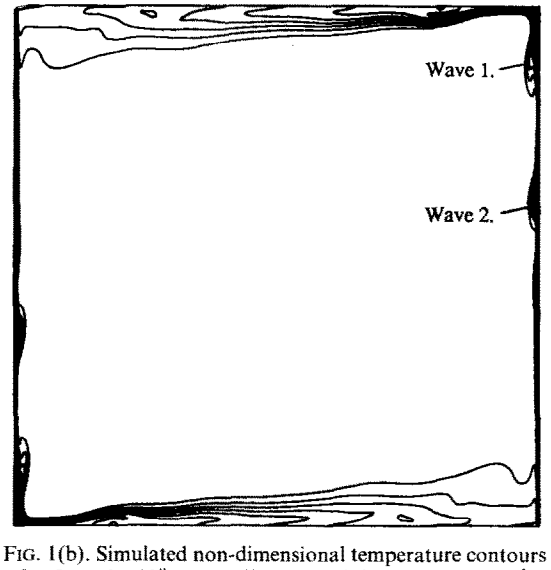

FIG. 1(b). Simulated non-dimensional temperature contours for $Ra = 5 \times 10^9$ at non-dimensional time $t = 1.0 \times 10^{-3}$.

Fig. 1(a); $Ra = 5 \times 10^9$, $t = 1.0 \times 10^{-3}$, Fig. 1(b)). The presence of the hot and cold intrusions at the top and bottom of the cavity is clear. The time presented in each case is such that the intrusion has just arrived at the far wall and two of the waves (marked) generated on the wall by this perturbation can be seen travelling away from the point at which the intrusion has struck. The first of these waves is about to reach the downstream end of the thermal boundary layer and enter the intrusion. A difference in amplitude in the waves is also clearly evident, with the wave closest to the downstream location being considerably larger than the trailing wave. As the waves increase in amplitude in the direction of travel additional peaks behind those two marked are not easily discerned, although at least one other is present. In addition, as the wavelength is approximately 0.3 of the cavity height, any single snap-shot will at most expose only three peaks. In both cases the intrusion temperature contours slope approximately uniformly from the inflow end of the intrusion to the far wall, corresponding to a piling up of the intrusion against the far wall boundary layer. The rapidly diverging flow region is also evident beginning at about $x = 0.9$ (a distance 0.1 from the beginning of the intrusion) and the associated peak at about $x = 0.8$ (a distance 0.2 from the beginning of the intrusion).

The waves observed in Fig. 1(b) may also be seen in Fig. 2, which shows the simulated temperature traces taken near the hot wall for $Ra = 5 \times 10^9$. The trace is taken at points a distance 0.004 in from the hot wall ($x = 0.996$) and at vertical locations $y = 0.25$ and 0.5. It is evident that there are two discrete periods of activity; the first immediately following start-up, and the second when the intrusion strikes the far wall. It is the second wave train that corresponds to the waves seen in Fig. 1(b). Each peak in the signal corresponds to the passage of a single wave crest past the position at which the trace is recorded. Thus the two crests visible in Fig. 1(b) correspond to the first two peaks in the second period of activity in Fig. 2. By considering the two traces in Fig. 2 it is evident once again that the amplitude of the wave increases with passage up the hot wall, and that as a result the number of discernible crests increases.

In Fig. 3 a result from the simulation of the $Ra = 6 \times 10^8$ case is compared to the corresponding experimental result obtained by ref. [5]. The temperature trace taken at $x = 0.996$ (0.004 in from the hot wall) and at mid-height, $y = 0.5$, is shown. The two periods of wave activity predicted by the simulation are also present in the experimental trace, indicating that they are indeed a genuine physical effect, rather than a spurious numerical feature. The simulation is leading the experiment slightly, which may be due to errors in the experimental apparatus resulting in a lower effective Rayleigh number. Despite this time lag and a slight discrepancy in amplitude, the simulation accurately predicts the occurrence and behaviour of the instability.

Figure 4 shows the temperature contours for both cases at later times than those shown in Fig. 1 ($Ra = 6 \times 10^8$, $t = 3.5 \times 10^{-3}$, Fig. 4(a); $Ra = 5 \times 10^9$, $t = 1.6 \times 10^{-3}$, Fig. 4(b)). Considerable changes are evident in these temperature fields when compared to those for the earlier times. Firstly, the temperature contours are now, in both cases, relatively flat, and secondly, a large perturbation is present at about the $x = 0.25$ location (a distance of 0.75 of the cavity width from the intrusion inflow corner). This perturbation and flattening of the isotherms is associated with the seiching effect of the fluid that has not been entrained by the far wall, and was observed piled up in Fig. 1. It is also apparent that the peak associated with the rapid flow divergence is now accentuated, and has shifted back towards the wall. The peak in both cases is located at approximately $x = 0.9$. For the higher Rayleigh number a mixing region is apparent inside the divergence, which is not present in the lower Rayleigh number flow. This is the only fundamental

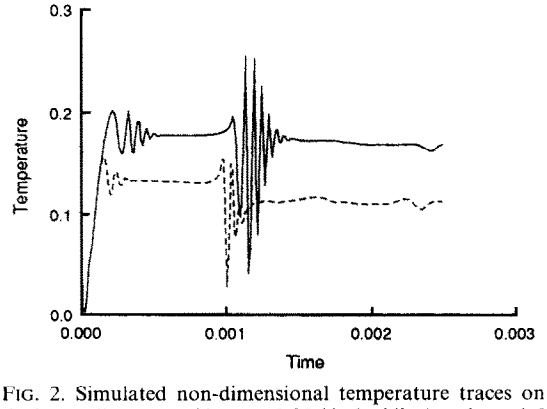

FIG. 2. Simulated non-dimensional temperature traces on the hot wall at $x = 0.996$, $y = 0.25$ (dashed line) and $y = 0.5$ (solid line) of the cavity width and height, for $Ra = 5 \times 10^9$.

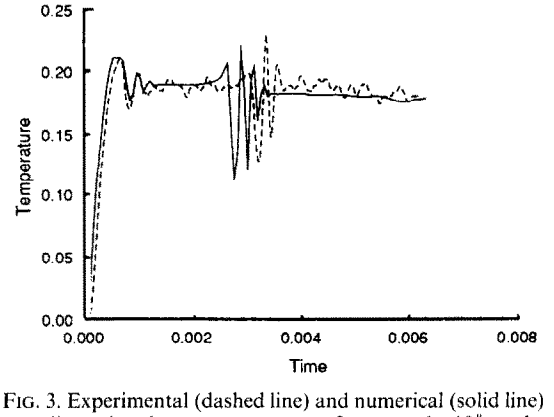

FIG. 3. Experimental (dashed line) and numerical (solid line) non-dimensional temperature traces for $Ra = 6 \times 10^8$ on the hot wall at $x = 0.996$ and $y = 0.5$ of the cavity width and height.

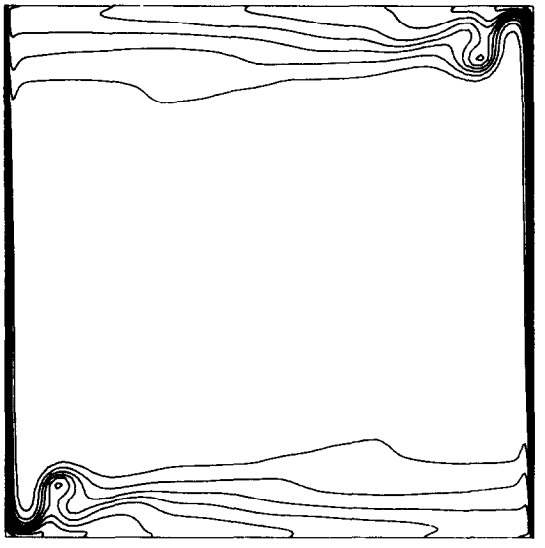

FIG. 4(a). Simulated non-dimensional temperature contours for $Ra = 6 \times 10^8$ at non-dimensional time $t = 3.5 \times 10^{-3}$.

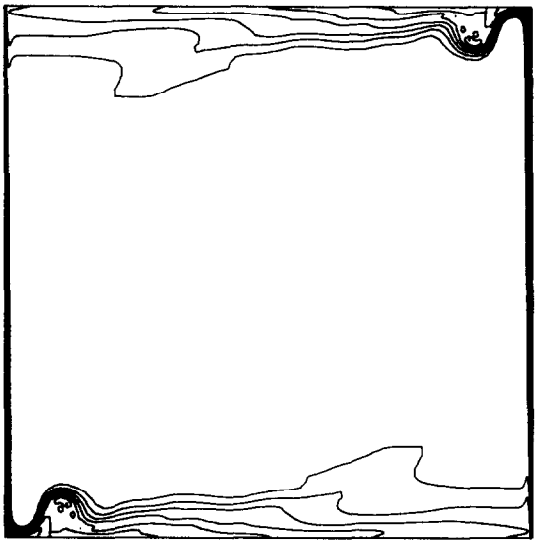

FIG. 4(b). Simulated non-dimensional temperature contours for $Ra = 5 \times 10^9$ at non-dimensional time $t = 1.6 \times 10^{-3}$.

difference between the results for the two Rayleigh numbers. Consistent with Fig. 2, there is no evidence of the travelling waves on the vertical boundary layers at these times.

Figures 5 and 6 give simulated temperature traces at three locations in the hot intrusion ($y = 0.95$) for the lower and higher Rayleigh numbers, respectively. In each figure, the x locations are 0.9, 0.5, and 0.1 in from the hot wall, recalling that the intrusion travels from right to left; that is from $x = 1.0$ to 0.0. The

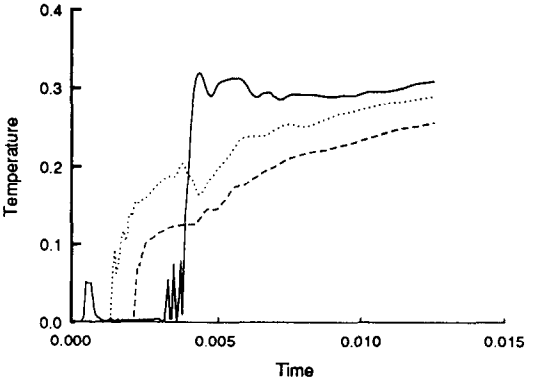

FIG. 5. Simulated non-dimensional temperature traces at $y = 0.95$ of the cavity height in the hot intrusion at $x = 0.9$ (solid line), $x = 0.5$ (dotted line) and $x = 0.1$ (dashed line) of the cavity width, for $Ra = 6 \times 10^8$.

$x = 0.9$ trace is located in the divergence peak for the later part of the record; for the earlier part, the location of this trace is outside the intrusion. Consider firstly Fig. 5. The two downstream traces ($x = 0.5$ and 0.1) show no signal until the nose of the initial intrusion passes by. The subsequent behaviour indicates weak wave activity at the mid point, and virtually no activity at the downstream end. The trace at $x = 0.9$ shows the passage of the intrusion nose and a weak indication of the first set of boundary generated waves, evident at this location at approximately $t = 2.5 \times 10^{-3}$, consistent with the evidence of Fig. 3. The second strong signal in the trace is associated with the second group of waves, at $t = 3.25 \times 10^{-3}$, and several distinct peaks are clearly evident. Following this, the divergence has moved back towards the corner, and the trace location is now within the intrusion flow. The sudden rise in temperature is followed by a group of longer period oscillations. In Fig.

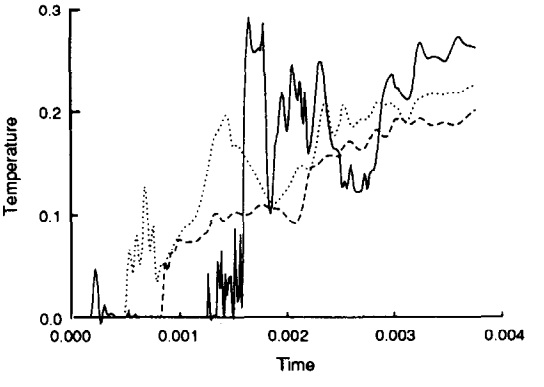

FIG. 6. Simulated non-dimensional temperature traces at $y = 0.95$ of the cavity height in the hot intrusion at $x = 0.9$ (solid line), $x = 0.5$ (dotted line) and $x = 0.1$ (dashed line) of the cavity width, for $Ra = 5 \times 10^9$.

6 ($Ra = 5 \times 10^9$) there are both similar and contrasting features. In common with the lower Rayleigh number case, the downstream traces show a marked reduction in activity. The upstream trace is also qualitatively similar for the early part of the record, although the start-up boundary layer waves are more clearly evident. Beyond the passage of the second group of waves however, the behaviour is much more complex, with apparently chaotic behaviour and activity spread across a broad spectrum of modes. This behaviour, although beginning at the time of arrival of the boundary layer waves, persists well beyond their passage. Evidently the divergence region has transited to an unstable regime.

The presence of the wave activity demonstrated in the temperature traces shown in Figs. 2, 3, 5 and 6 is best quantified by spectral methods. Plots of the two sided power density spectrum against wave number (2π frequency) are given, where the power density spectrum is obtained by squaring the modulus of the Fourier transform. For $Ra = 6 \times 10^8$, the power spectra for the simulated trace shown in Fig. 3 and the upstream trace shown in Fig. 5 are shown in Fig. 7. Figure 7(a) gives the spectrum for the signal in the thermal boundary layer ($x = 0.996$, $y = 0.5$, corresponding to the simulated result shown in Fig. 3), and Fig. 7(b) shows the power spectrum for the signal in the inflow region of the hot intrusion ($x = 0.9$, $y = 0.95$, corresponding to the solid line in Fig. 5). The thermal boundary layer signal spectrum (Fig. 7(a)) shows a clear peak at a wave number of 3.0×10^4, corresponding to the waves occurring at start-up and at $t = 2.5 \times 10^{-3}$ which have (from Fig. 3) a period of approximately 2.1×10^{-4}. The spectrum for the intrusion signal (Fig. 7(b)) contains the same clear single peak. Evidently no additional modes have been added to the signal in its passage through the divergence.

In contrast however, the spectra from the corresponding locations in the high Ra case (Figs. 8(a) and (b), corresponding to the solid line traces shown in Figs. 2 and 6) are markedly different in character. The thermal boundary layer signal (Fig. 8(a)) shows a clear peak at a wave number of 1.26×10^5, corresponding to the waves of period 5.0×10^{-5} generated in the layer at start-up and at $t = 1.0 \times 10^{-3}$. In the intrusion, however, there is no such distinct peak, and energy is present over a wide spectrum of wave numbers, both higher and lower than the original value in the vertical layer. This suggests that energy from the divergence is passing into a broad spectrum of wave numbers. This is fundamentally a different behaviour to the lower Ra case, and is consistent with the presence of the mixing patch in the divergence in the high Ra case. As the signals analysed are of short duration, it is not possible to draw conclusive results from the spectral analysis; the results are however indicative of the behaviour, and give support to conclusions that may be drawn from inspection of the raw data.

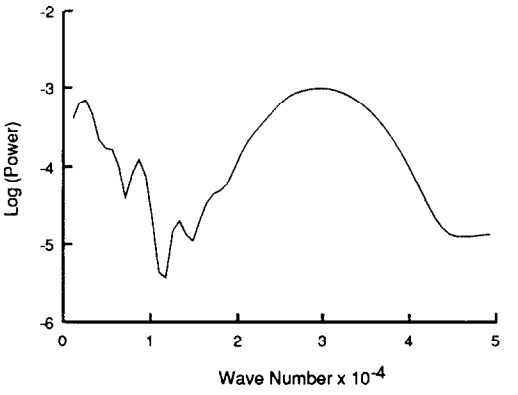

FIG. 7(a). Non-dimensional power spectrum for simulated non-dimensional temperature trace on the hot wall at $x = 0.996$ and $y = 0.5$ of the cavity width and height with $Ra = 6 \times 10^8$.

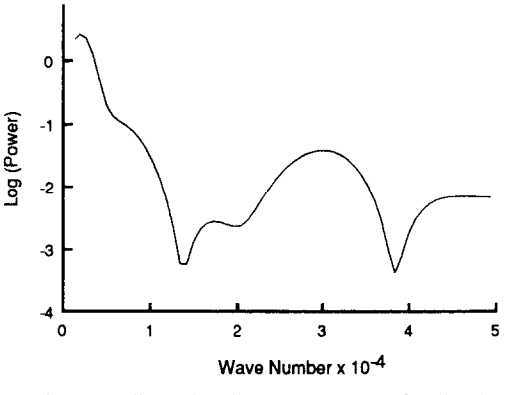

FIG. 7(b). Non-dimensional power spectrum for simulated non-dimensional temperature trace in the hot intrusion at $x = 0.9$ and $y = 0.95$ of the cavity width and height with $Ra = 6 \times 10^8$.

3.1. *Internal wave*

The Nusselt number at the cavity centreline for the $Ra = 6 \times 10^8$ flow as a function of time is shown in Fig. 9. The signal consists of a base low wave number signal, with a superimposed high wave number signal in the first peak and trough. The first high wave number signal is produced by the start-up boundary layer wave travelling across the intrusion, and the second by the waves resulting from the intrusion striking the far wall. This result indicates that at least some of the energy in the boundary layer wave is available at the mid point of the cavity. The amplitude and period of the low wave number signal reduces with time. The reduction in amplitude is most apparent in the first three peaks, with the period dropping from 2.3×10^{-3} to 1.0×10^{-3} over the trace given. The low wave number signal seen is evidently the result of the cavity scale seiching with the decrease in period resulting from the

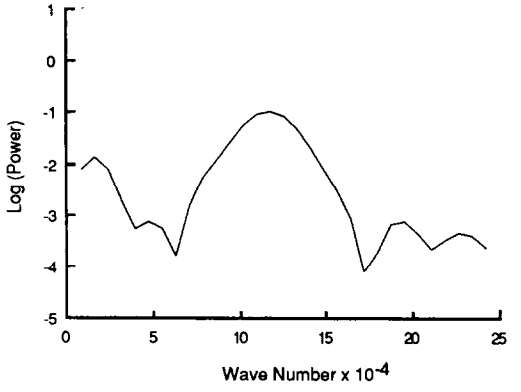

FIG. 8(a). Non-dimensional power spectrum for simulated non-dimensional temperature trace on the hot wall at $x = 0.996$ and $y = 0.5$ of the cavity width and height with $Ra = 5 \times 10^9$.

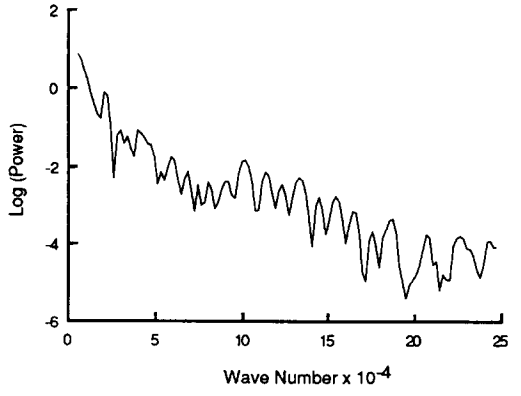

FIG. 8(b). Non-dimensional power spectrum for simulated non-dimensional temperature trace in the hot intrusion at $x = 0.9$ and $y = 0.95$ of the cavity width and height with $Ra = 5 \times 10^9$.

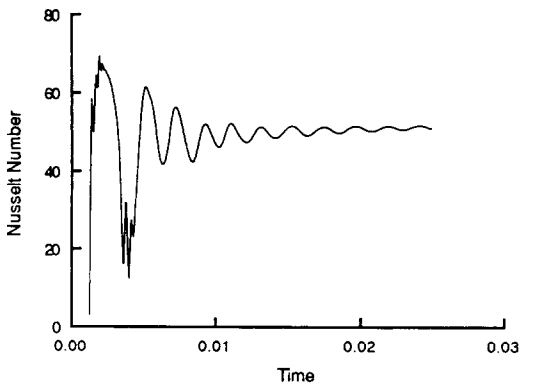

FIG. 9. Simulated Nusselt number at the centreline for $Ra = 6 \times 10^8$.

change in stratification from effectively a three-layer system, that is an isothermal core with the hot and cold intrusions, to quasi-linear as the cavity core fills from above and below with heated and cooled fluid from the intrusions. The reduction in amplitude suggests that the wave results from a single perturbation rather than a continuous energy input.

The temperature traces at $x = 0.5$, where the Nusselt number is calculated, do not show a strong indication of the cavity scale waves (Fig. 5). This means that the variation in the Nusselt number is due primarily to an oscillating advection effect. This is demonstrated in Fig. 10, which shows the time dependence of the horizontal velocity component at $x = 0.75$, 0.5, and 0.25 in the hot intrusion ($y = 0.95$). The signals shown are taken after the passage of the second set of boundary generated waves. There are clearly a number of low wave number signals present, and in particular, the low wave number mode present in the Nusselt number calculation is also present in the $x = 0.5$ signal. This signal may also be observed, in phase, in the other traces, although, consistent with this being a first mode oscillation, the signal is strongest at the cavity mid point. Additional higher mode activity is also present; this dies away rapidly as expected and towards the end of the signal only the first mode low wave number signal is clearly present.

Figure 11 shows the simulated temperature trace on the hot wall at $x = 0.996$ (a distance 0.004 in from the hot wall) and $y = 0.75$ after the passage of the second set of waves. The figure shows recurring periods of high wave number activity superimposed on the longer period waves. This activity correlates with the forward surges of the intrusion as indicated in Fig. 10. It therefore appears that the cavity scale wave by itself perturbs the boundary layer enough to produce the travelling wave instability. However, it is also apparent that the amplitude of these waves is much smaller than those produced by the initial striking of

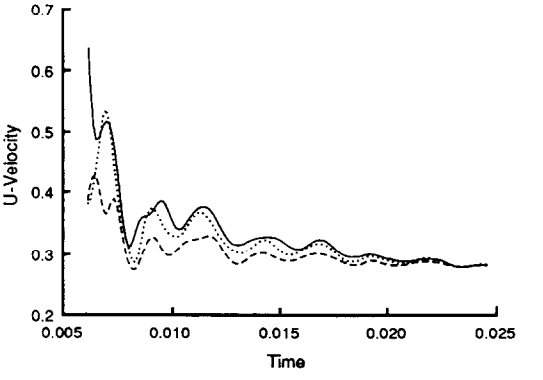

FIG. 10. Simulated absolute horizontal non-dimensional velocity traces in the hot intrusion at $y = 0.95$ of the cavity height and $x = 0.75$ (dashed line), $x = 0.5$ (dotted line), $x = 0.25$ (solid line) of the cavity width, for $Ra = 6 \times 10^8$.

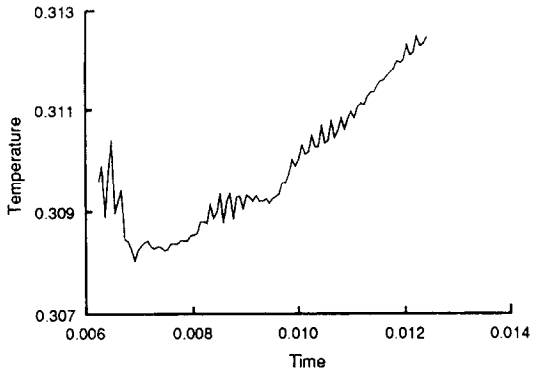

FIG. 11. Amplification of the simulated non-dimensional temperature trace on the hot wall at $x = 0.996$ and $y = 0.75$ of the cavity width and height with $Ra = 6 \times 10^8$.

the far wall by the intrusion; consequently they do not produce the peaks seen in the temperature contours in Fig. 1, and without the amplification used in this figure would not be readily discernible. This aspect has not been pursued in the present paper.

4. DISCUSSION

4.1. *Boundary layer instability*

Results have been presented demonstrating that a travelling wave instability in the boundary layer occurs at both start-up time and when the intrusion striking the far wall perturbs the boundary layer, for Rayleigh numbers of 6×10^8 and 5×10^9. The effect is stronger at the higher Rayleigh number. The travelling wave is observed to increase in amplitude in its direction of travel, up the hot wall and down the cold wall, and then to dissipate after travelling part way across the intrusion.

Consider first the set of waves occurring at start up. The occurrence of such waves in natural convection flows on vertical plates is well known and has been studied extensively, both experimentally and analytically. In a recent paper by Joshi and Gebhart [13], experimental results are presented for the natural convection flow of water on a constant heat flux vertical plate. The behaviour of the temperature traces at start up is identical to that presented here. Initially, the temperature increases smoothly to a value greater than the steady-state value, a series of decaying oscillations follow, and finally a steady state is reached.

The observed behaviour whereby the temperature initially overshoots the steady-state value is described by the similarity solutions to the boundary layer equations for flow on a semi-infinite instantaneously heated vertical flat plate, obtained by Brown and Riley [14], and in more detail by Williams *et al.* [15]. These analyses demonstrate that the boundary layer has three regions. Nearest to the leading edge of the plate is a steady-state region in which the horizontal conduction of heat from the plate into the fluid is balanced by the transport of cooler entraining fluid into the boundary layer. Far downstream from the leading edge is a region where there is no entrainment and the temperature field behaves as a solution to the one-dimensional horizontal conduction equation. A transition region connects these two regions. At the intersection of the transition and conduction regions is a singularity, generated at the leading edge of the plate at time $t = 0$ due to the step function increase in temperature. As the flow develops this singularity travels up the plate away from the leading edge.

The singularity occurs in the similarity solution only because it is obtained from the boundary layer equations in which the stream-wise diffusion terms have been dropped. Physically, and in the solution to the full equations, the point will not be a singularity but will be associated with a rapid, though not instantaneous, change in the flow.

If the penetration distance of the temperature field is greater than the steady-state thermal boundary layer thickness by the time the singularity arrives at a given vertical location, then the observed overshoot will occur, and the final approach to steady state will be from above, rather than from below as might be expected.

Additionally it has been demonstrated by Gebhart and Mahajan [16], and others, that for the Rayleigh numbers considered the boundary layer is unstable to travelling waves at specific frequencies. These features allow the observed behaviour of the cavity flow at start-up to be described in the following way. The observed overshoot in the temperature field occurs due to the relation between the time scale of the one-dimensional conduction equation and the speed of travel of the singularity described above. The singularity itself will be represented by an infinite number of wave number components. The boundary layer will act to selectively amplify the wave number component for which it is unstable and thus the singularity is observed travelling up the plate with a stationary, with respect to the singular point, trailing wave train. At a fixed vertical location this is seen as a decaying oscillation as the temperature transits from the overshoot value to the steady-state value. This behaviour is consistent with that observed on a vertical plate at start-up.

Gebhart and Mahajan [16] present a formula for the characteristic wave number of the boundary layer for the flat plate flow of the form

$$\text{wave number} = \frac{0.3\nu}{\delta_1 4^{1/4} Gr^{1/12}}.$$

Using this formula with the scalings given by Gebhart and Mahajan gives a predicted wave number of 3.14×10^4 for the low Ra and 1.3×10^5 for the high Ra, as compared to the simulated results of 3.0×10^4 and 1.26×10^5. The predictions are in both cases very close to the simulation values, providing further sup-

port that the simulated waves are of the same type as those occurring on the flat plate.

LeQuere and Alziary de Roquefort [8] also observed waves of this type in natural convection in rectangular cavities. In that case both pure conductive and insulated boundary conditions for the horizontal boundaries were considered. For the adiabatic boundary conditions waves were only observed for aspect ratios (height/width) of greater than two, occurring above a critical Rayleigh number of 1.5×10^7. Rather than solving the stationary initial value problem as in this paper, in ref. [8] solutions were obtained by perturbing steady flows with a sudden increase in Rayleigh numbers. The result was the presence of waves in a periodically steady flow that persisted over long integration times, in the presence of a stable linear background stratification. The flow is therefore substantially different to that in which the waves arise in the present investigation; here the waves are a transient phenomenon occurring early in the flow, when the background stratification is zero. However, the appearance and description of the waves given in ref. [8] suggest they are of the same type observed in the present case.

Although the indications are that the initial set of waves occurring on the vertical wall in the simulations presented in this paper are identical in their generation mechanism to those observed with the flat plate, the second set of waves cannot be described in exactly the same way. The waves occurring at start-up are associated with a perturbation over the entire wall, and the subsequent passage of the leading edge singularity, a global perturbation. The intrusion produces only a local perturbation to the boundary layer, the extent of which is determined by the intrusion thickness.

The intrusion effectively perturbs the boundary layer to a higher Rayleigh number structure, due to a combination of the lower temperature and the higher entrainment velocity. The transition is accomplished once again in an oscillatory fashion at the characteristic frequency of the boundary layer, associated with the passage of a singularity from the bottom to the top of the perturbation region. The resultant waves continue to travel through the remainder of the boundary layer, as observed.

After the initial arrival of the intrusion subsequent forward surges will not bring significant changes in temperature, and thus the only perturbation effect will be that associated with the change in entrainment velocity, which will be smaller than that associated with the initial combined effect of temperature and velocity. For this reason, the initial arrival of the intrusion causes the greatest effect, although as has been shown subsequent velocity surges do produce, albeit significantly weaker, travelling wave instabilities each time the boundary layer is compressed.

4.2. *Intrusion divergence response*

At the larger of the two Rayleigh numbers the divergence region exhibits complex behaviour during and after the arrival of the travelling waves. The temperature signal (Fig. 6) contains a broad spectrum of modes, both higher and lower than the boundary layer wave mode.

The face of the divergence evidently steepens as a result of the seiche arising from the intrusion striking the far wall, and the complex signal observed could be attributed to either or both the travelling waves and the seiche. The steepening of the face of the divergence due to the seiche will increase the likelihood of it becoming unstable. Further, in the lower Rayleigh number case the travelling waves do not produce a similar response. It seems likely therefore that the response is due to the increase in steepness resulting from the seiche.

Paolucci and Chenoweth [7] postulate, after Ivey [6], that the divergence is an internal hydraulic jump. The Froude number of the intrusion inflow upstream of the divergence is 0.7 for the lower Rayleigh number and 1.4 for the higher, based on the calculation of mean velocities and temperatures over the width of the intrusion. Additionally the divergence behaviour has been observed for flows with an internal Froude number of 0.1. This suggests that the divergence is not an internal hydraulic jump in the usual sense.

It does appear, however, that the value of the Froude number is important in determining the behaviour of the divergence crest. In this way it is exhibiting surface jump-like behaviour, where for Froude numbers of between 1 and 1.3 a surface jump will exist with a stationary trailing wave train acting to dissipate energy, and for Froude numbers above 1.3 the jump will foam, with energy being dissipated in the resultant turbulent structure. For Froude numbers of less than 1 a jump cannot exist. The act of a surface jump foaming is similar to that of any gravity wave breaking, and is primarily linked to the steepness of the face of the wave.

In the present case if the divergence peak is considered to be a standing gravity wave, then the effect of the seiche is to dramatically steepen the face of that wave. For the lower Rayleigh number, and hence lower Froude number, the intrusion is able to respond in a way that precludes breaking by its ability to dissipate energy against the direction of the flow. For the higher Rayleigh number, higher Froude number flow, this is not possible, and as a result the face of the peak steepens until it begins to break, generating the observed mixing patch in the region of the divergence. It is suggested that this is an analogue of the foaming of surface hydraulic jumps, although the behaviour of an internal density wave will be different to that of one occurring at an air–water interface.

The amplitude of the divergence is increased and its face steepened by the seiche effect resulting from the far wall, and as this also generates the travelling wave instabilities, the face is steepening just at the time the waves from the boundary layer are arriving. Energy can no longer be dissipated smoothly and a mixing patch, by which energy is dissipated, occurs within the

divergence. After the passage of the travelling waves the face is further steepened by the seiche, and a continuation of the mixing behaviour is observed.

This behaviour is only observed in the higher of the two Rayleigh number flows, indicating that it has in some sense crossed a stability threshold. It appears that the stability threshold is related to the Froude number being greater than 1.0. It should be noted that in the present case the peak required the additional steepening resulting from the seiche to become unstable. Possibly at higher Rayleigh numbers the phenomenon would occur without the additional steepening resulting from the seiche. This speculation has not been pursued.

4.3. *Internal waves*

The low wave number signal may be identified as a cavity scale seiching motion from the results for the horizontal velocity in the intrusion. These demonstrate that the signal is in phase over the intrusion, and that it is strongest at the centre, with an approximately equal drop in strength on both sides. A second mode signal, strongest at the $\frac{1}{4}$ and $\frac{3}{4}$ width locations, is the first harmonic of the cavity scale. Higher modes may be present, but are not clearly identifiable from the results. As expected, the first harmonic is observed to dissipate faster than the cavity scale seiche.

The frequency of the seiche is observed to increase with the filling of the core region of the cavity with heated and cooled fluid. Initially, the core region essentially comprises three layers of fluid; a stratified intrusion, an unstratified core, and another stratified intrusion. As the cavity fills the thickness of the unstratified core reduces, and ultimately a quasi-linear stratification results. The period of the simulated cavity scale oscillation (for $Ra = 6 \times 10^8$) in the later part of the record, when the fluid is closer to a linear stratification, is approximately 1.0×10^{-3}, whilst in the initial stages the period is approximately 2.3×10^{-3}, more than twice its final value.

The first mode internal wave solution for the linear stratification, based on the full temperature difference from top to bottom of the cavity [1], is easily shown to have a period of 9.6×10^{-4}, very close to the value obtained from the later part of the simulation. For an idealized three layer structure, that is, linearly stratified intrusions each of thickness 0.08 and an unstratified core with each intrusion containing one half of the full temperature difference, numerical solution of the appropriate one-dimensional wave equation yields a period of 1.9×10^{-3}, again similar to the value obtained above for the early part of the simulation. The hypothesis that the low wave number oscillations observed are first mode internal waves is strongly supported by these results.

The results also indicate that the cavity scale signal is present everywhere in the intrusion, although slightly stronger in the region of the divergence. In this region the velocity gradients are greater than in other regions of the intrusion, and the effect of a cavity scale signal will be amplified.

Paolucci and Chenoweth [7] also observe that the signal is stronger in the divergence region, and interpret this to mean that the divergence is driving the seiche. This would suggest that the divergence had a natural frequency that exactly matched that of the cavity, and varied in the manner observed for the variation in the cavity scale signal.

Any perturbation is capable of generating the seiche, and the crossing of the cavity by the intrusion is such a perturbation. In addition, the intrusion cannot be fully entrained by the far wall, as it is the fluid which is not entrained that provides the heated and cooled fluid for the core region of the cavity. As the fluid that is not entrained may only be dispersed as a gravity wave at the cavity seiche scale, it is clear that the effect of the intrusion striking the far wall will be to generate a cavity scale seiche. The energy in the seiche will then be dissipated in the normal way by viscous forces.

Although it is possible that additional energy goes into the cavity scale wave from the divergence, as suggested by ref. [7], in the absence of evidence to suggest otherwise, the scenario above seems a more natural one for the cavity scale wave generation.

5. CONCLUSIONS

A time-accurate second-order implicit code has been applied to the problem of unsteady natural convection in a cavity with differentially heated side walls. The code may be used with a non-staggered mesh without the accompanying problem of pressure splitting due to the inclusion of regularizing terms in the Poisson pressure equation.

Comparison between experimental and numerical results has demonstrated that the code is capable of accurately predicting the occurrence of a travelling wave instability in the wall thermal boundary layers for natural convection in a cavity. The occurrence of such a feature has been predicted by ref. [9] and others. The waves are observed to travel at approximately the peak local advective velocity, and to increase in amplitude in the direction of travel.

The onset of the instability in each case is caused by a significant perturbation to the boundary layer. In the present case the perturbations are caused by the initial start-up, and by the intrusion striking the far wall. The waves travel along the vertical wall and into the intrusion, where they dissipate without reaching the far wall. If they were to reach the far wall it is possible that they would continue into the far wall boundary layer, leading to a self-sustaining periodic flow. Such a flow has been observed by ref. [8], although as described previously the method of obtaining the flow is quite different to that used in the present investigation.

It is clear from the results presented that the response of the intrusion to the instability, for the

higher Rayleigh number at least, is quite complex. However, in both cases the travelling waves dissipate rapidly and therefore do not reach the far side of the cavity.

Ivey [6] postulated that the complex flow structure observed in the inflow region of the intrusion was an internal hydraulic jump, based on the observation that for the Rayleigh number considered the intrusion inflow had a Froude number greater than one. It was also suggested that the observed high wave number activity was generated by the jump. As seen in the results shown in the present paper the divergence with the associated peak will occur even for a Rayleigh number in which the Froude number is less than unity, indicating that it cannot be an internal hydraulic jump in the usual sense. Additionally, it appears that the occurrence of the boundary layer instability is independent of the divergence region of the intrusion.

A cavity scale seiche is observed at both the Rayleigh numbers considered. Paolucci and Chenoweth [7] suggest that this internal wave is generated by the divergence in the intrusion, which they identify as a hydraulic jump, after ref. [6]. Further, ref. [7] discounts the intrusion overshoot suggested by ref. [1] as a possible generation mechanism.

There are a number of problems with this hypothesis, which is based on surface hydraulic jump arguments. Surface hydraulic jumps exist in either foaming ($Fr > 1.3$) or stationary downstream wave train ($1.0 < Fr < 1.3$) regimes. The hypothesis assumes that at the higher Froude number a jump will exhibit the first mode seiche frequency, however there is no evidence that this is the case for either a surface or internal hydraulic jump. In particular, the foaming regime is, as the name implies, chaotic, with no periodically steady low-wave number signal being present. In addition, as has been demonstrated here, at the lower Rayleigh number the divergence cannot be a jump in the usual sense, and yet the cavity seiche signal is still evident.

It is therefore suggested that the seiche results from the perturbation to the system caused by the observed overshoot of the intrusion when it strikes the far wall.

Paolucci and Chenoweth [7] further suggest that at sufficiently high Rayleigh number the flow will branch to a fully chaotic solution due to the suggested internal hydraulic jump mechanism. This is essentially saying that the jump, if it exists, transits to the equivalent of the foaming regime for sufficiently high values of Ra. Although on the basis of the present investigation the jump mechanism cannot provide a total explanation for all of the observed features, it appears that the analogy is useful in explaining the observed mixing region of the divergence for the higher Rayleigh number flow. In a surface hydraulic jump the foaming ultimately occurs because the face becomes too steep. Here the interaction of the seiche and the divergence leads to a steepening of the face, following which the mixing behaviour occurs. This suggests that when the Froude number is greater than 1 the face of the divergence becomes sufficiently steep for the observed behaviour to occur. The idea of breaking resulting from face steepening will apply to any gravity wave, and the jump analogy is not the only one that can be drawn.

This implies that the hydraulic jump analogy is useful and meaningful in aiding the understanding of the mixing behaviour in the intrusion divergence, and it is likely, as refs. [6, 7] suggest, that at high Rayleigh numbers this mechanism will lead to the flow becoming fully turbulent in this region. It appears doubtful that the jump argument can be used to explain the cavity scale seiching motion that may be more simply explained by the observed intrusion overshoot. Likewise, the jump argument cannot explain the travelling waves on the walls and resulting high wave number activity which result from perturbations to the thermal boundary layer, and which are also a potential cause of the transition to turbulence.

Finally, the influence of the presence of both the travelling wave instabilities and the cavity scale seiching on the heat transfer properties is clear from Fig. 9. The net heat transfer, as measured by the Nusselt number, approaches steady state in a decaying oscillatory fashion as the result of the cavity scale seiche, on which are superimposed the high frequency signals from the boundary layer waves. As the amplitude of the Nusselt number oscillation at early time is not significantly less than the steady-state value, the engineering implications of the presence of these effects may be significant, particularly if the forcing of the system, that is the time scale of the application of the horizontal temperature difference, is similar to the time scale of the Nusselt number oscillations.

Acknowledgement—The authors wish to thank Jorg Imberger, Charles Jeeveraj, John Taylor and Greg Ivey for their useful suggestions. This research was supported by the Australian Research Council in the form of a National Research Fellowship and by grant A48615453, and the Australian Water Research Advisory Council.

REFERENCES

1. J. C. Patterson and J. Imberger, Unsteady natural convection in a rectangular cavity, *J. Fluid Mech.* **100,** 65–86 (1980).
2. P. M. Gresho, R. L. Lee, S. T. Chan and R. L. Sani, Solution of the time-dependent incompressible Navier–Stokes and Boussinesq equations using the Galerkin finite element method. In *Approximation Methods for Navier–Stokes Problems* (Edited by R. Rautmann), Springer Lecture Notes in Mathematics, Vol. 771, pp. 203–222 (1980).
3. B. Staehle and E. Hahne, Overshooting and damped oscillations of transient natural convection flows in cavities, 7th Int. Heat Transfer Conf., Munich (1982).
4. S. G. Schladow, J. C. Patterson and R. L. Street, Transient flow in a side-heated cavity at high Rayleigh number, *J. Fluid Mech.* **200,** 121–148 (1989).
5. J. C. Patterson and S. W. Armfield, Transient features of natural convection in a cavity, *J. Fluid Mech.* **219,** 469–497 (1990).
6. G. Ivey, Experiments on transient natural convection in a cavity, *J. Fluid Mech.* **144,** 389–401 (1984).

7. S. Paolucci and D. R. Chenoweth, Transition to chaos in a differentially heated vertical cavity, *J. Fluid Mech.* **201,** 379–410 (1989).
8. P. LeQuere and T. Alziary de Roquefort, Transition to unsteady natural convection of air in differentially heated vertical cavities, *Numerical Methods in Laminar and Turbulent Flow, Proc. 4th Int. Conf.*, Swansea, pp. 841–852 (1985).
9. A. E. Gill and A. Davey, Instabilities of a buoyancy driven system, *J. Fluid Mech.* **35,** 775–798 (1969).
10. S. V. Patankar, *Numerical Heat Transfer and Fluid Flow*. Hemisphere, Washington, DC (1980).
11. S. W. Armfield, Finite difference solutions of the Navier–Stokes equations on staggered and non-staggered grids, *Computational Techniques and Applications : CTAC 89*, Brisbane, pp. 289–294. Hemisphere (1990).
12. B. P. Leonard, A stable and accurate convective modelling procedure based on quadratic upstream interpolation, *Comp. Meth. Appl. Mech. Engng* **19,** 59–98 (1979).
13. Y. Joshi and B. Gebhart, Transition of vertical natural convection flows in water, *J. Fluid Mech.* **179,** 407–438 (1987).
14. S. N. Brown and N. Riley, Flow past a suddenly heated vertical plate, *J. Fluid Mech.* **59,** 225–237 (1973).
15. J. C. Williams, J. C. Mulligan and T. B. Rhyne, Semi-similar solutions for unsteady free convective boundary layer flow on a vertical flat plate, *J. Fluid Mech.* **175,** 309–332 (1987).
16. B. Gebhart and R. L. Mahajan, Instability and transition in buoyancy induced flows, *Adv. Appl. Mech.* **18,** 231–315 (1982).

SIMULATION DIRECTE DES INTERACTIONS D'ONDES POUR LA CONVECTION NATURELLE VARIABLE DANS UNE CAVITE

Résumé—Des solutions numériques pour la convection naturelle instationnaire dans une cavité carrée avec des parois chauffées différemment sont obtenues en utilisant un schéma implicite de volumes finis et elles sont comparées à des données expérimentales antérieures. Les résultats prédisent l'apparition d'une oscillation, la présence d'ondes dans la couche limite thermique verticale qui traversent depuis la paroi et une région de forte divergence à l'extrémité des intrusions. On observe trois mécanismes qui interfèrent à un nombre de Rayleigh de 5×10^9 pour produire une configuration de mélange dans l'intrusion, ce qui suggère une transition vers la turbulence. Le transfert thermique et l'approche de l'état stationnaire sont fortement influencés par la présence des ondes.

DIREKTE SIMULATION VON WELLENÜBERLAGERUNGEN BEI DER NICHTSTATIONÄREN NATÜRLICHEN KONVEKTION IN EINEM HOHLRAUM

Zusammenfassung—Die nichtstationäre natürliche Konvektionsströmung in einem quadratischen Hohlraum mit unterschiedlich beheizten Seitenwänden wird numerisch unter Verwendung eines impliziten zeitgenauen Finite-Volumina-Verfahrens zweiter Ordnung untersucht. Ein kurzer Vergleich mit früher veröffentlichten Versuchswerten schließt sich an. Die Ergebnisse sagen das Auftreten einer sogenannten Seiche im gesamten Hohlraum voraus: dies sind Wellen in der senkrechten thermischen Grenzschicht, welche von den Wänden in das Gebiet der waagerechten Begrenzungen eindringen, wobei ein Gebiet großer Verstärkung am stromauf gelegenen Ende dieser Eindringzone auftritt. Es wird beobachtet, daß diese drei Mechanismen bei einer Rayleigh-Zahl von 5×10^9 in der Weise zusammenwirken, daß sich im Eindringgebiet eine Mischzone ergibt, was schließlich einen Übergang zur Turbulenz hervorruft. Der Netto-Wärmeübergang und die Annäherung an den stationären Zustand werden sehr stark vom Vorhandensein der Wellen beeinflußt.

НЕПОСРЕДСТВЕННОЕ МОДЕЛИРОВАНИЕ ВОЛНОВЫХ ВЗАИМОДЕЙСТВИЙ ПРИ НЕСТАЦИОНАРНОЙ ЕСТЕСТВЕННОЙ КОНВЕКЦИИ В ПОЛОСТИ

Аннотация—С использованием неявной трехмерной схемы второго порядка точности по времени получены численные решения для нестационарной естественной конвекции в квадратной полости с различно нагретыми боковыми стенками, и проведено их краткое сравнение с имеющимися в литературе экспериментальными данными. Полученные результаты предсказывают существование сейша масштаба полости, наличие волн в вертикальном тепловом пограничном слое, волн, удаляющихся от стенок к горизонтальным интрузиям, образующимся на горизонтальных границах, и область сильной расходимости в направленном против течения крае интрузий. При числе Рэлея величиной 5×10^9 наблюдается взаимодействие трех указанных механизмов, в результате которого в интрузии образуется участок смешения, где, по-видимому, происходит переход к турбулентности. Результирующий теплоперенос и приближение к стационарному состоянию в значительной мере зависят от наличия волн.